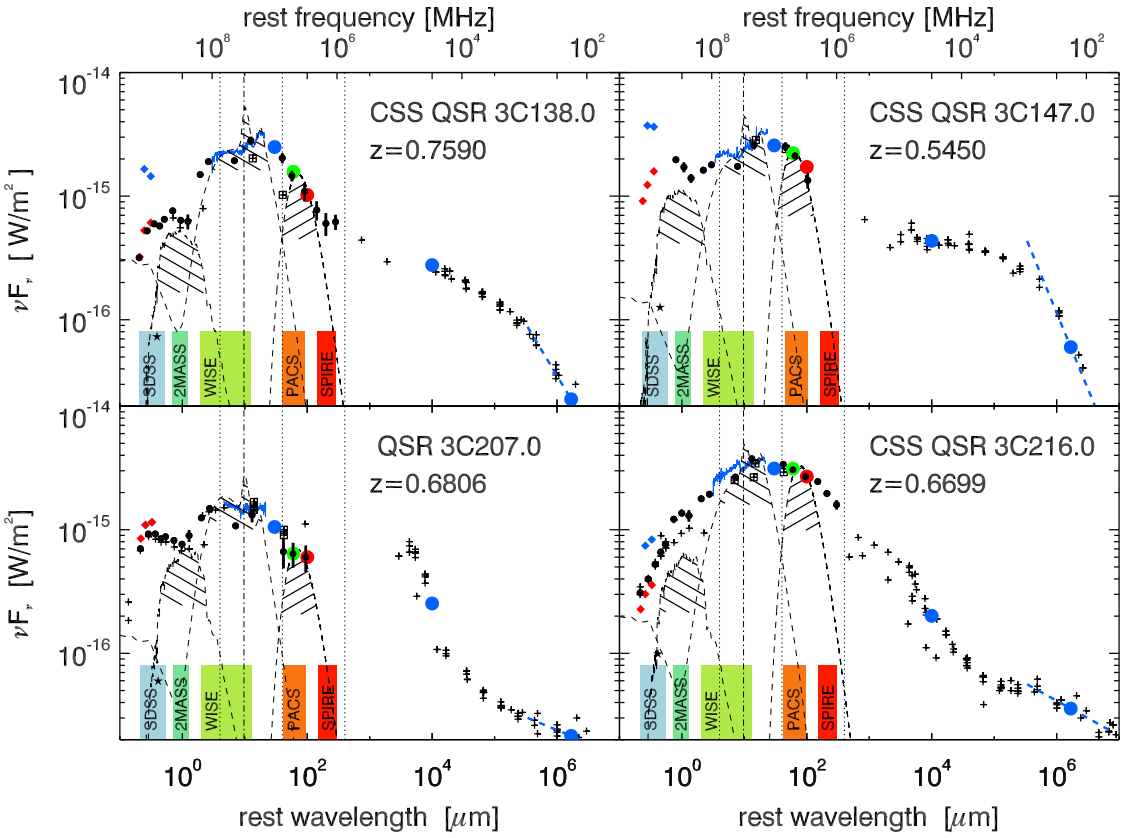

Fig. 1.— Spectral energy distributions of 4 flat spectrum quasars (FSQs) at $0.5 < z < 1$, i.e. quasars where the GHz respectively cm spectrum rises towards shorter wavelengths in νF_ν scaling. Filled black circles with error bars denote detections, 3σ upper limits are marked by arrows. The Herschel PACS and SPIRE band ranges are shadowed in red, the 2MASS and WISE ranges in green, the optical (SDSS) range in blue. Red and blue diamonds are optical photometry values from Véron-Cetty and Véron (2010) and from Laing *et al.* (1983)), respectively. "+" symbols are detections (with arrows: upper limits) collected via NED. Disentangled host flux from Lehnert *et al.* (1999) is shown with a star symbol. Black open squares mark photometry with Spitzer/MIPS at 24 μm or Spitzer/IRS; IRS spectra are plotted as blue lines and the position of the 9.7 μm silicate absorption is indicated by the black vertical dash–dotted line. SCUBA 450/850 μm and IRAM 1.2 mm data points by Haas *et al.* (2004) are marked with black dots. Large blue dots mark median data points at 30 GHz and 178 MHz restframe. Big blue, green and red dots at IR-wavelengths mark interpolated flux levels at 30, 60 and 100 μm, respectively. Models of the host galaxy, the AGN heated warm dust and the SF heated cool dust are shown as dashed lines.

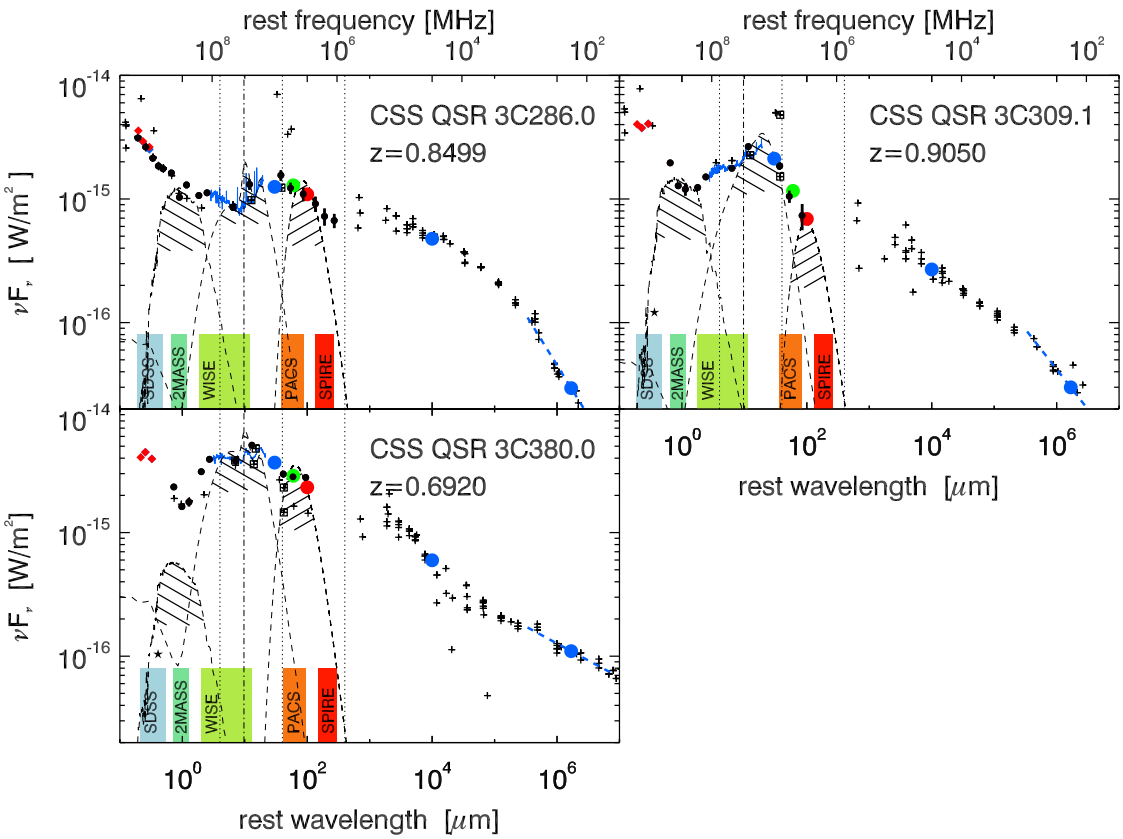

Fig. 1.— continued

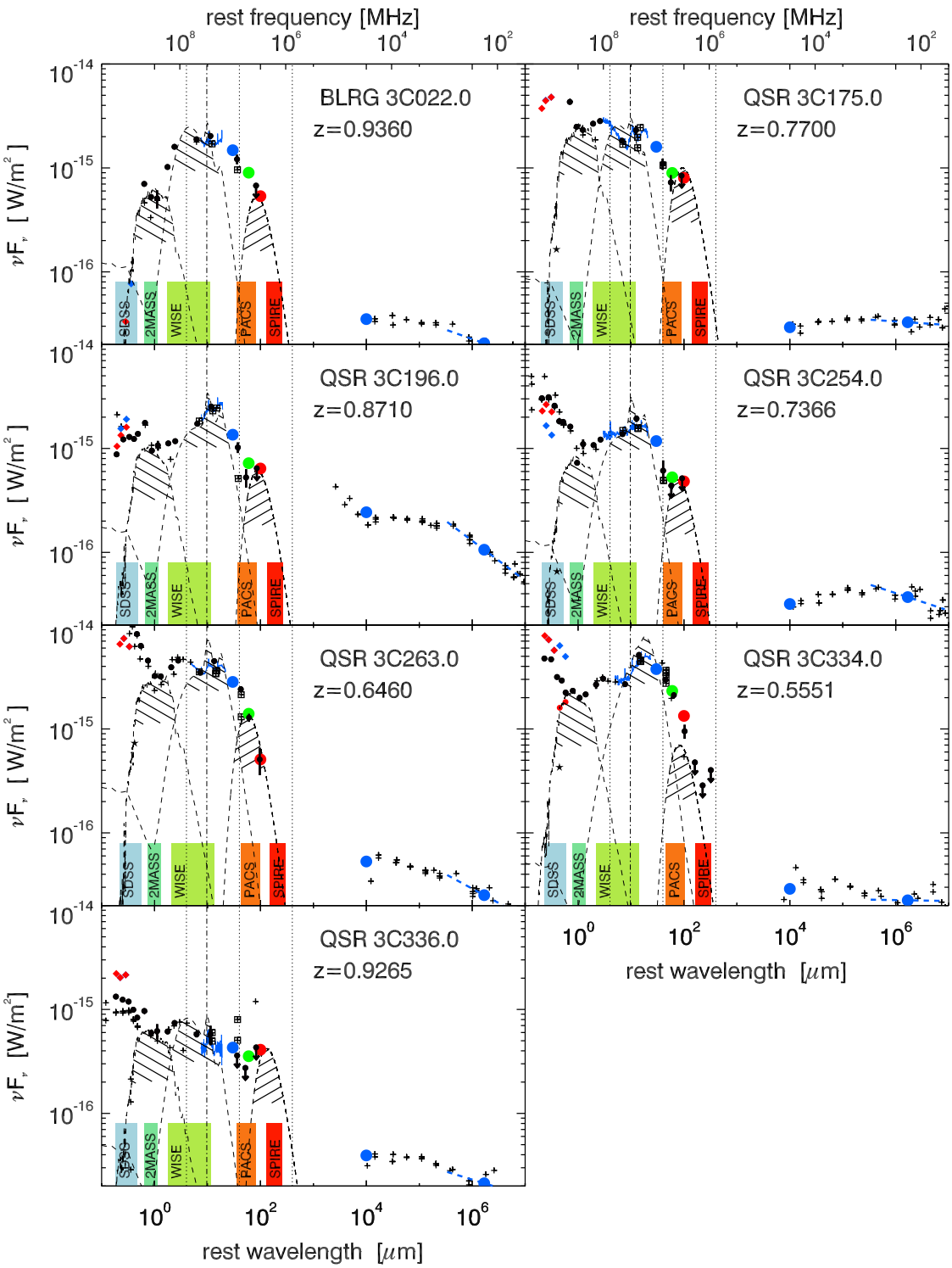

Fig. 2.— Spectral energy distributions of 6 steep spectrum quasars (SSQs) at $0.5 < z < 1$, with strong optical AGN continuum and one BLRG without strong optical AGN continuum. Notation as in Fig.1.

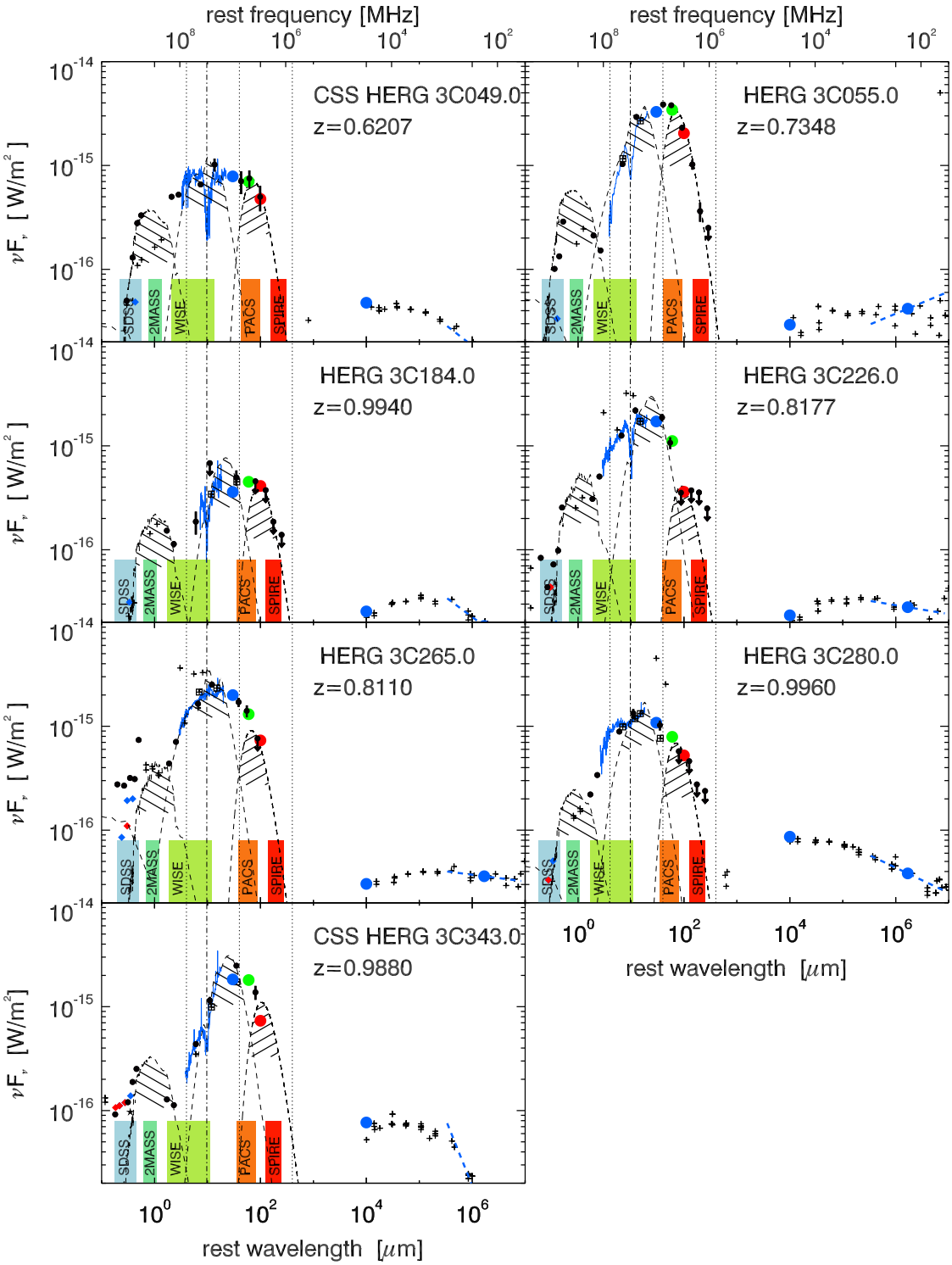

Fig. 3.— Spectral energy distributions of high excitation radio galaxies (HERGs) at $0.5 < z < 1$, with bright MIR emission, up to a factor ten above the host galaxy level. Note the deep 9.7 μm silicate absorption in the CSS 3C 49 and in 3C 55, 3C 226 and 3C 343. Notation as in Fig.1.

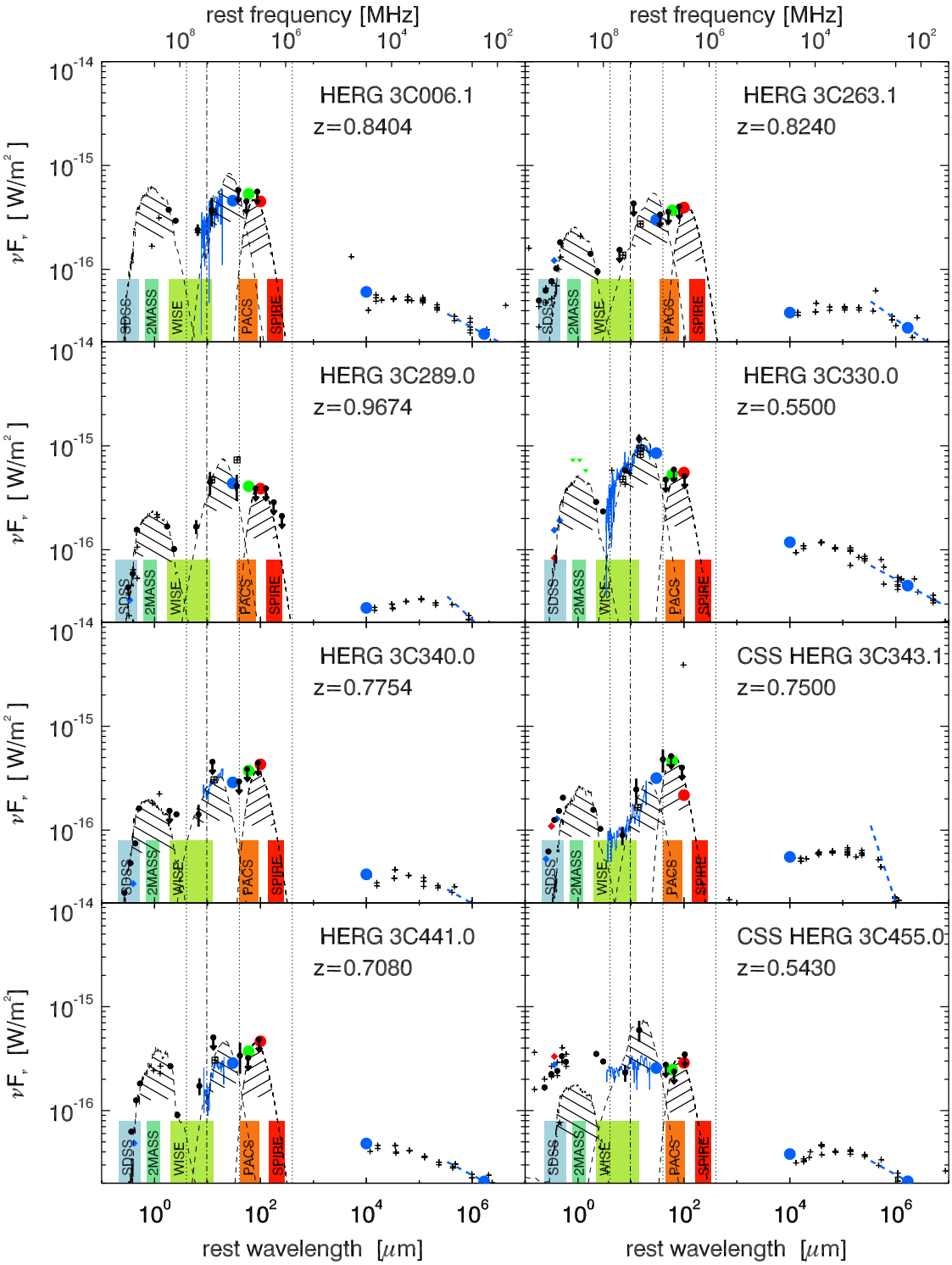

Fig. 4.— Spectral energy distributions of high excitation radio galaxies (HERGs) at at $0.5 < z < 1$, with medium MIR emission, reaching at about 30 μm the host galaxy level. Note the valley of low $4 - 10$ μm emission in most sources. 3C 330 and 3C 441 are the only sources with successfully measured 9.7 μm silicate absorption. Notation as in Fig.1.

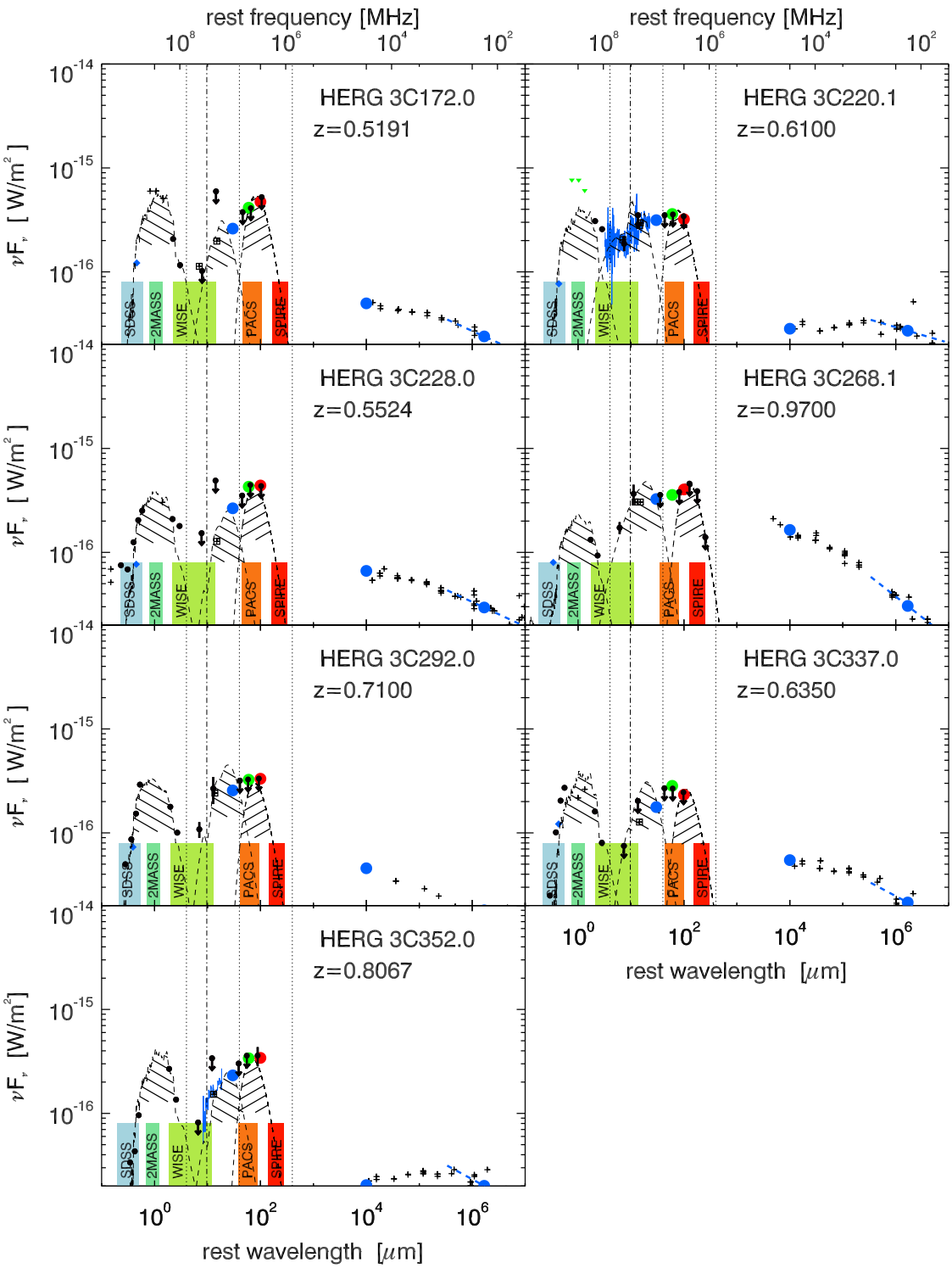

Fig. 5.— Spectral energy distributions of HERGs at $0.5 < z < 1$, with weak MIR emission. All sources have a low $4 - 10$ μm emission and barely reach at about 30 μm the host galaxy level. Notation as in Fig.1.

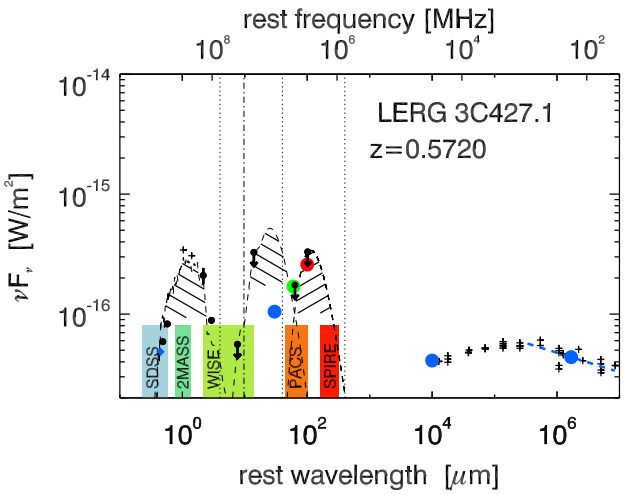

Fig. 6.— Spectral energy distributions of the only LERG in our sample at $0.5 < z < 1$. Note the low MIR flux compared to the host flux. Notation as in Fig.1.

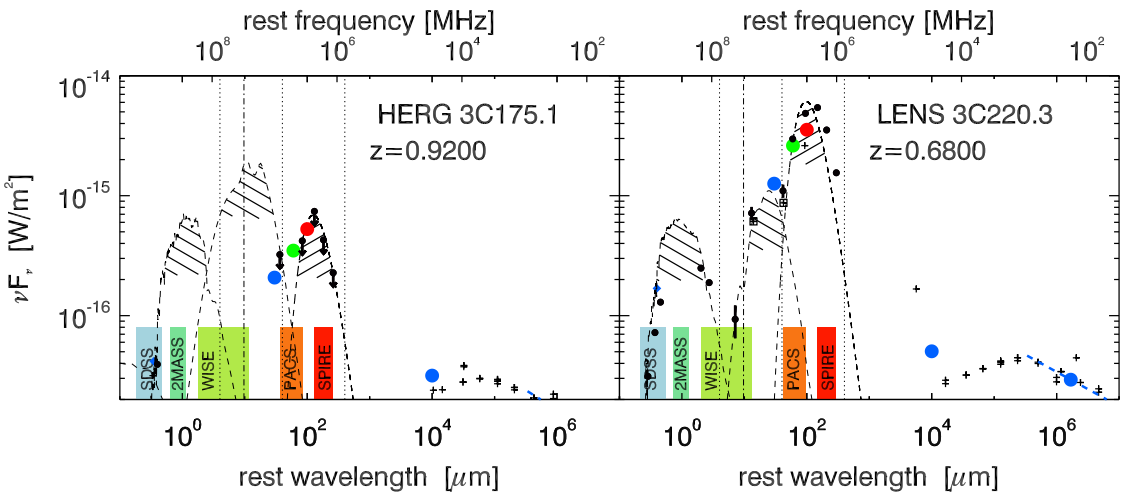

Fig. 7.— Spectral energy distributions of two HERGs at $0.5 < z < 1$, which have been excluded from the analysis. 3C 175.1 has too few data points and 3C 220.3 shows excess FIR-submm emission due to a gravitationally lensed submillimetre galaxy at z=2.2 (Haas et al. 2014). Notation as in Fig.1.

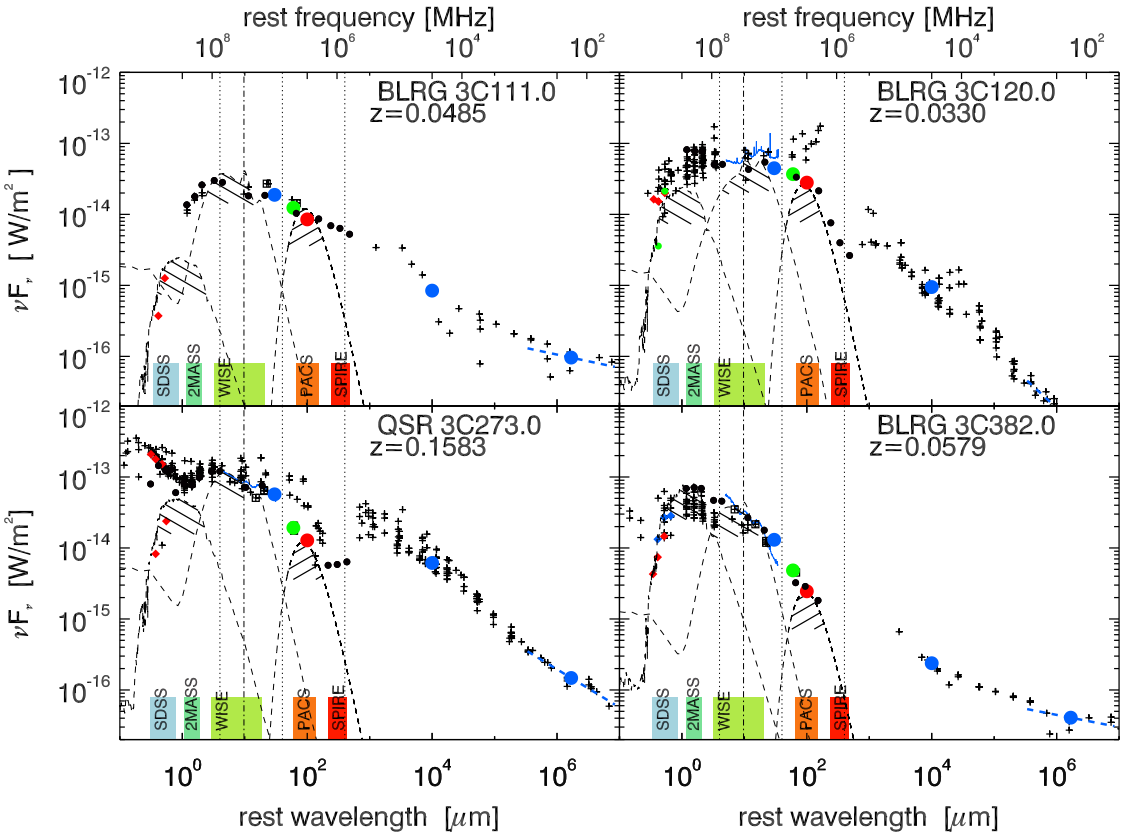

Fig. 8.— Spectral energy distributions of the flat spectrum sources at $z < 0.5$, three BLRGs and one quasar. Notation as in Fig.1.

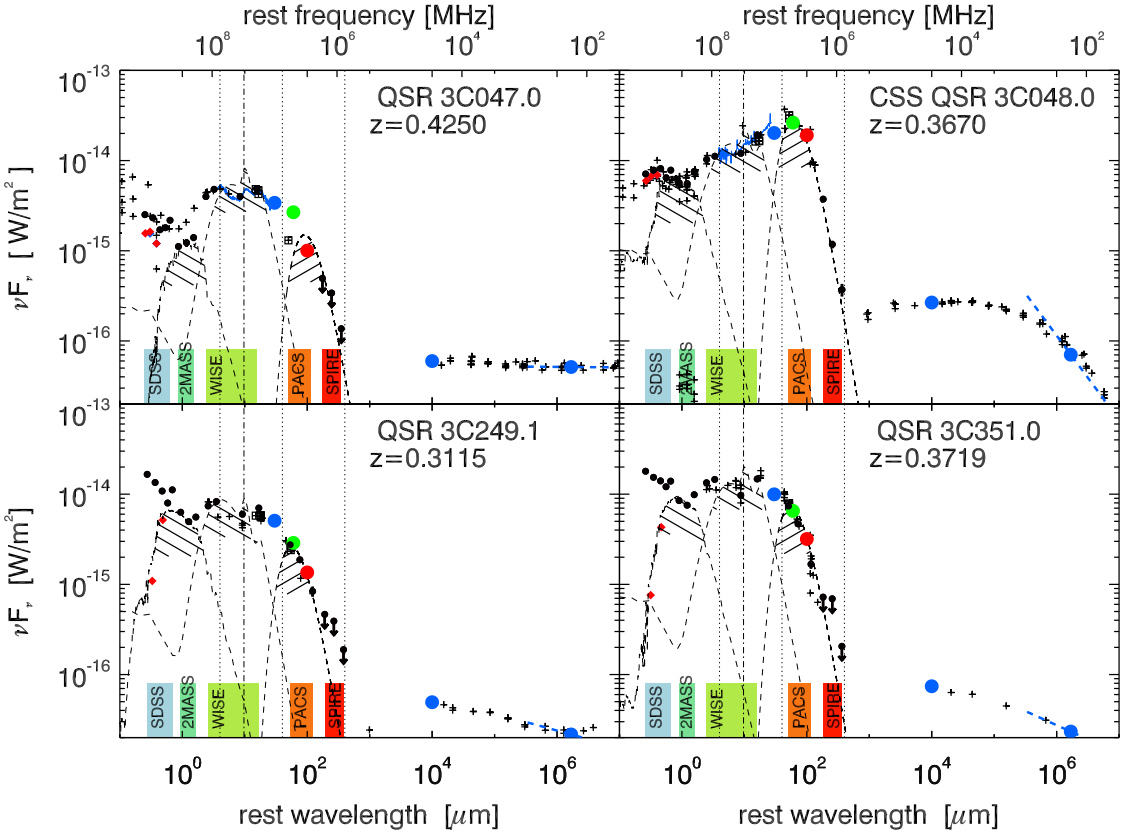

Fig. 9.— Spectral energy distributions of steep spectrum quasars at $z < 0.5$. Notation as in Fig.1.

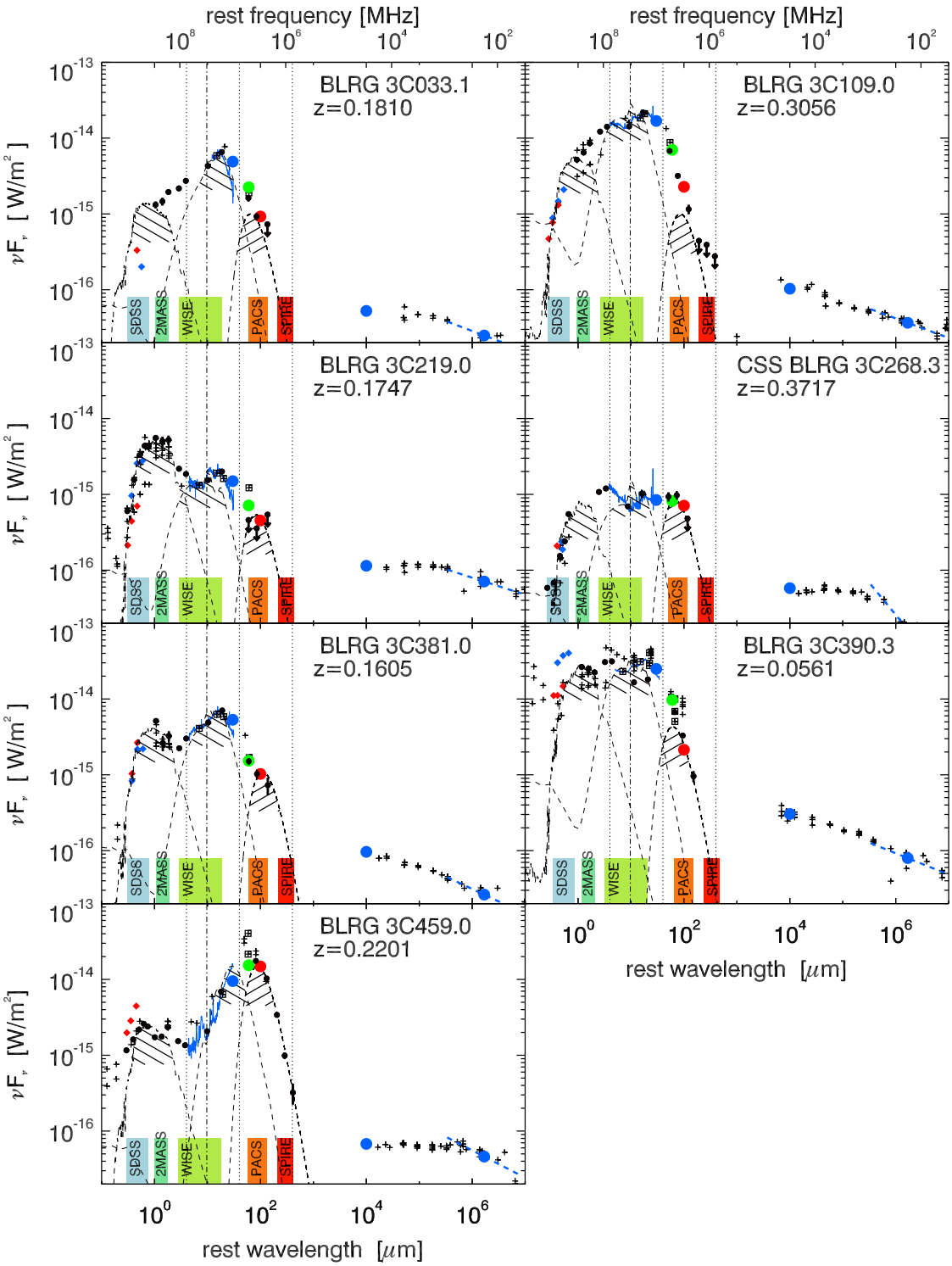

Fig. 10.— Spectral energy distributions of steep spectrum BLRGs at $z < 0.5$. Notation as in Fig.1.

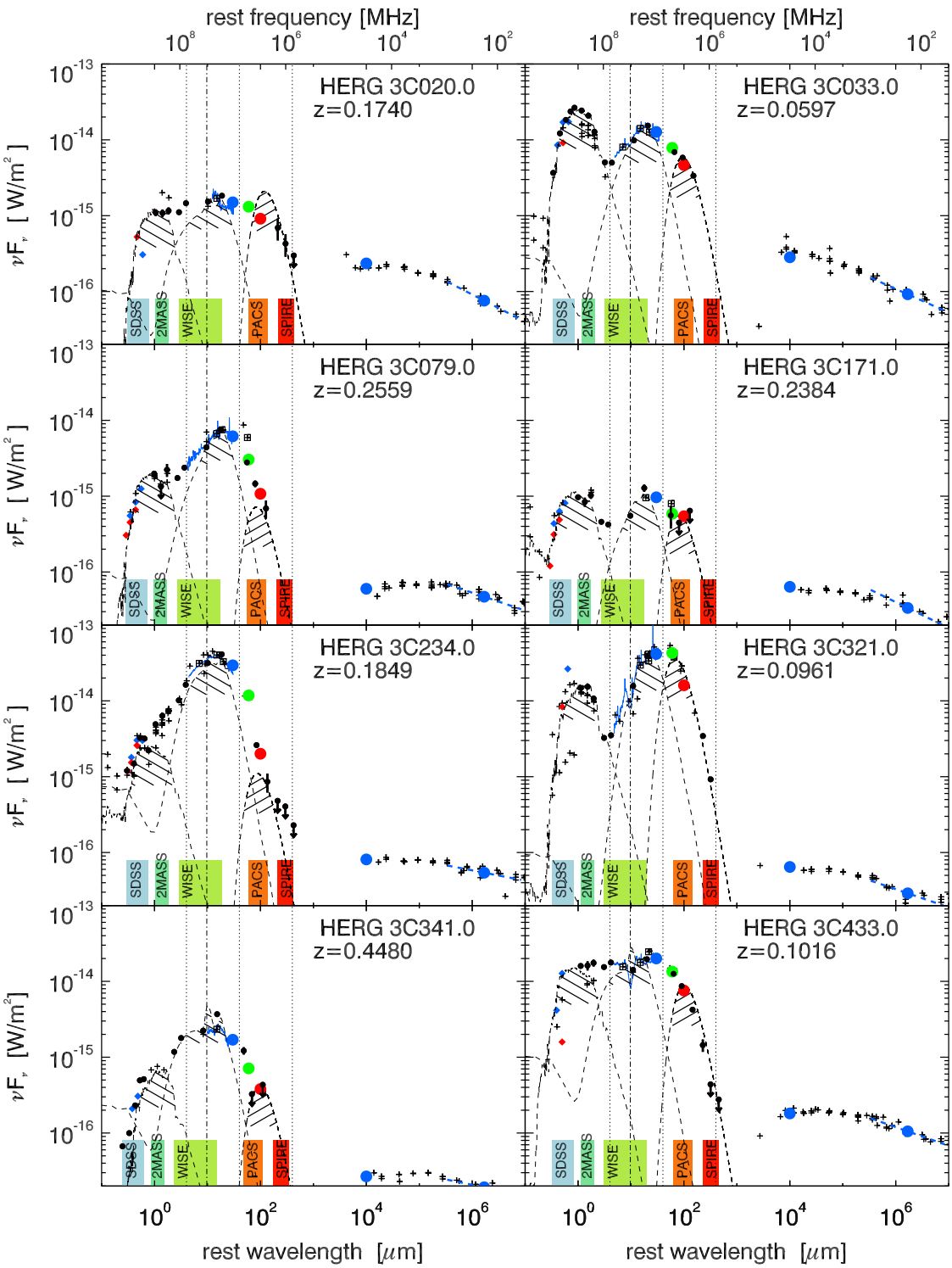

Fig. 11.— Spectral energy distributions of high excitation narrow line radio galaxies with strong MIR emission at $z < 0.5$. Notation as in Fig.1.

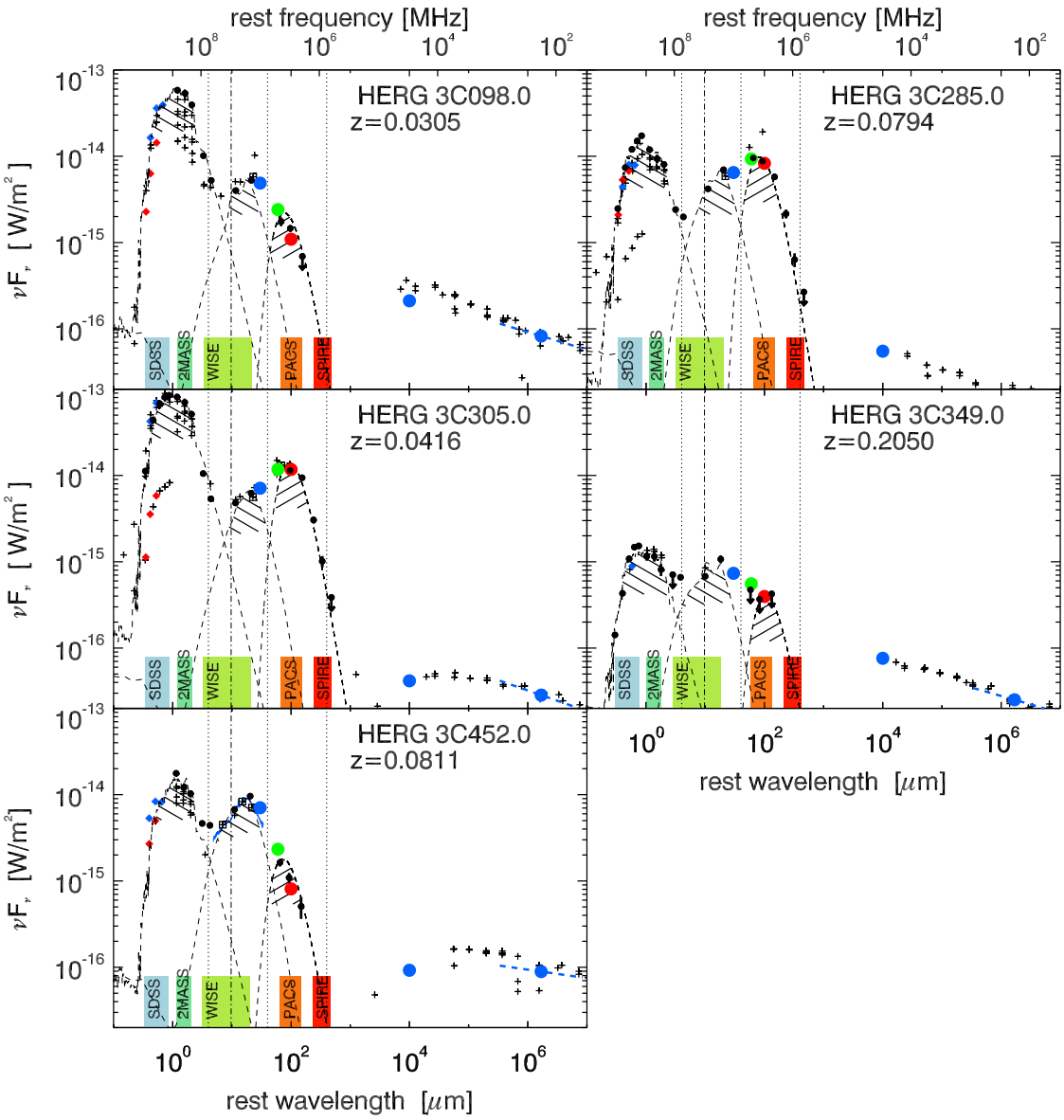

Fig. 12.— Spectral energy distributions of high excitation narrow line radio galaxies with medium MIR emission at $z < 0.5$. Notation as in Fig.1.

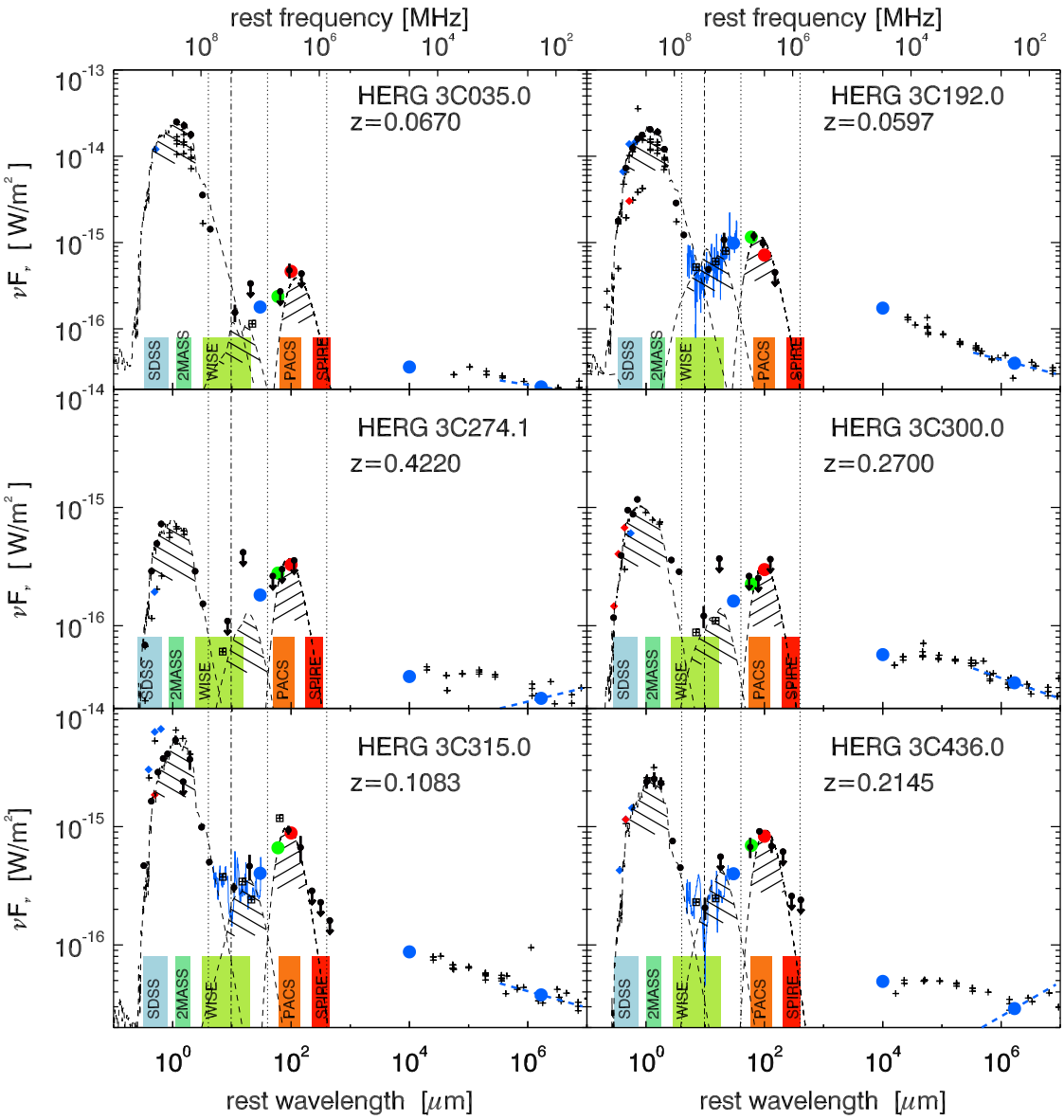

Fig. 13.— Spectral energy distributions of high excitation narrow line radio galaxies with weak MIR emission. Notation as in Fig.1.

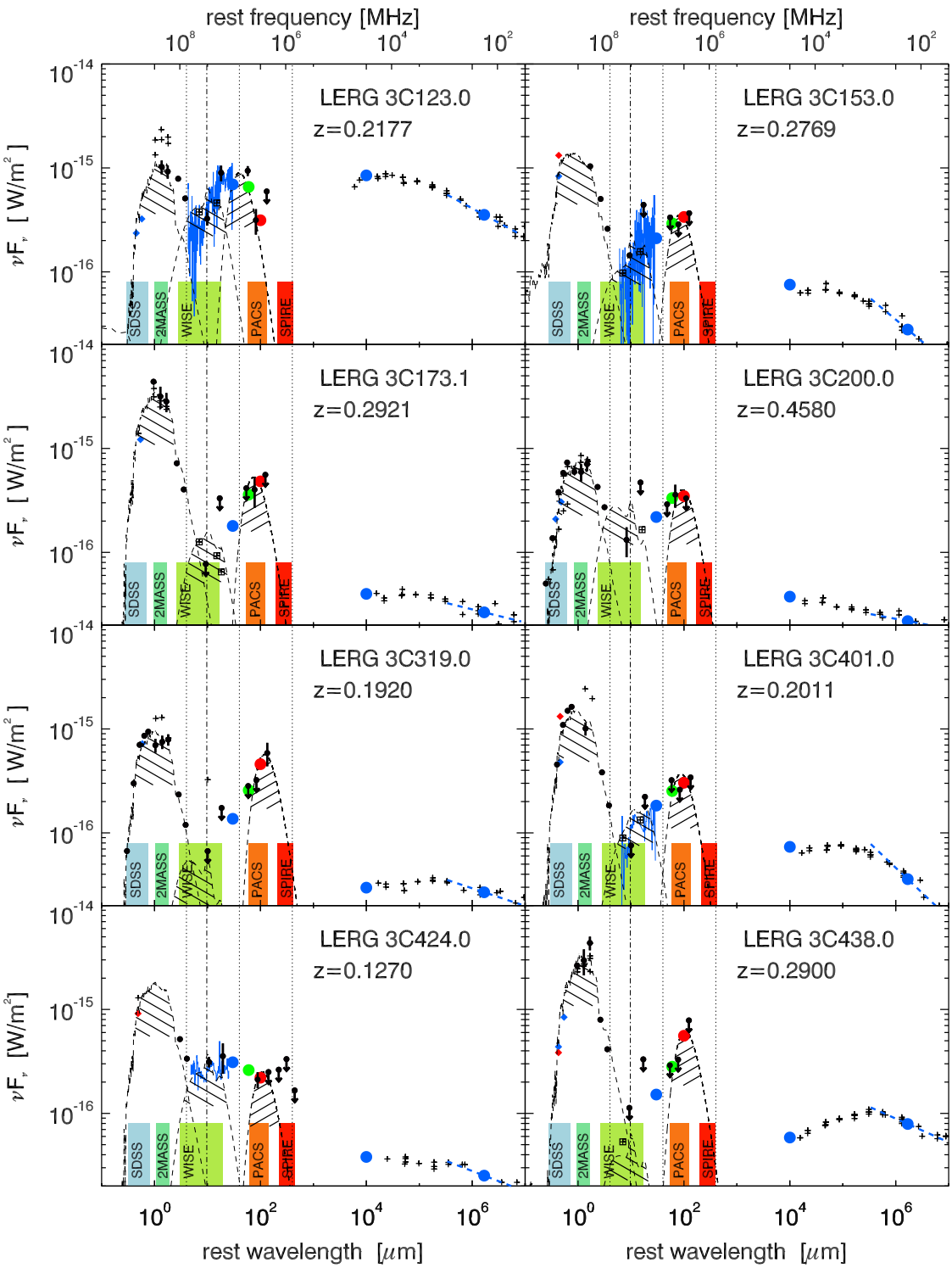

Fig. 14.— Spectral energy distributions of low excitation narrow line radio galaxies (LERGS) at $z < 0.5$. Notation as in Fig.1.

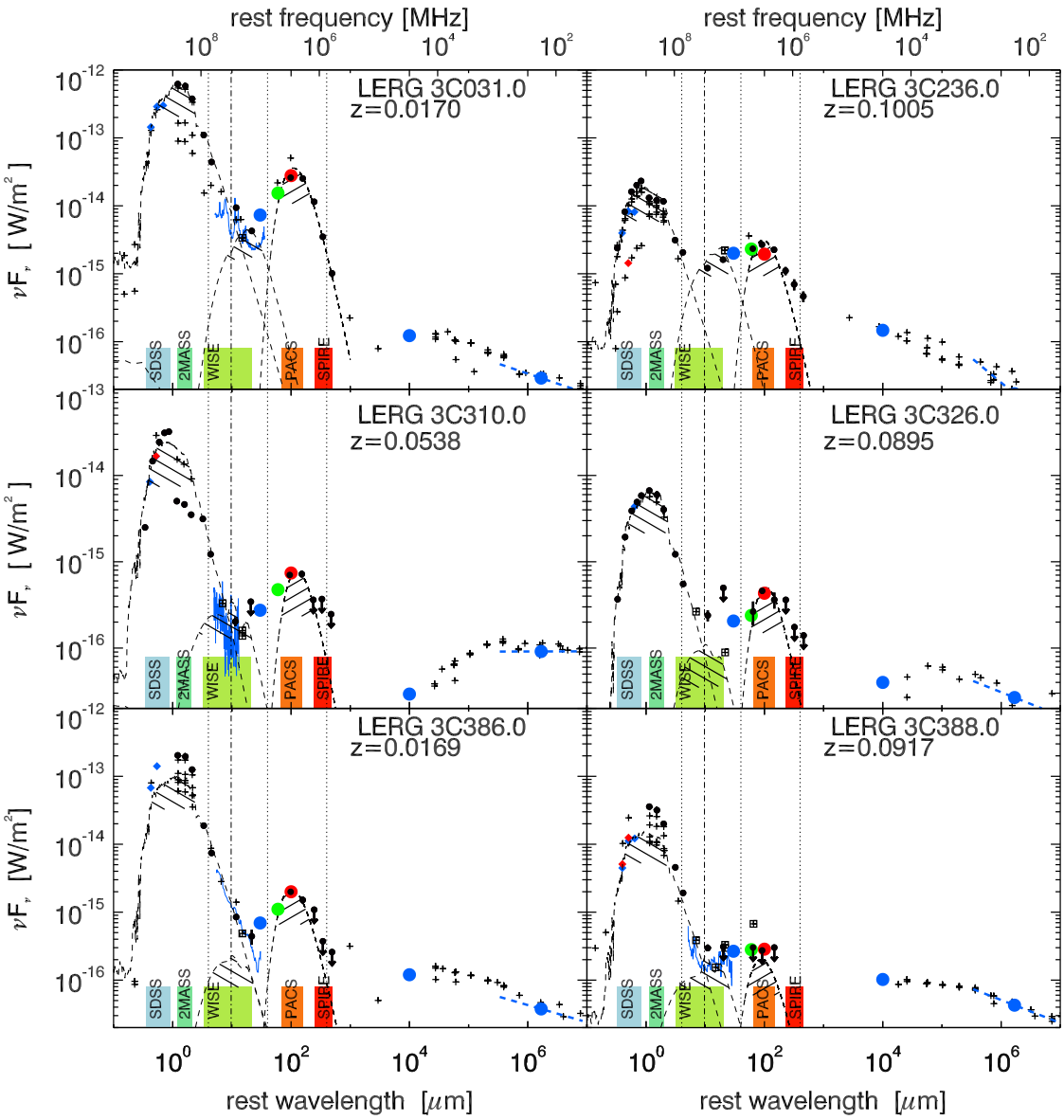

Fig. 15.— Spectral energy distributions of LERGS, with very low $L_{\rm MIR}/L_{\rm Host}$ at $z < 0.5$. Notation as in Fig.1.